Available online at www.sciencedirect.com
SCIENCE DIRECT®
ELSEVIER
Coastal Engineering 49 (2003) 239–261
Coastal Engineering
An International Journal for Coastal, Harbour and Offshore Engineers
www.elsevier.com/locate/coastaleng

Moving shoreline boundary condition for nearshore models

R.S. Prasad, I.A. Svendsen*

Department of Civil Engineering, College of Engineering, CACR, University of Delaware, 137 DuPont Hall, Newark, DE 19716, USA

Received 3 June 2002; received in revised form 23 April 2003; accepted 4 June 2003

Abstract

The paper develops and analyzes two fully nonlinear boundary conditions that incorporate the motion of the shoreline in nonlinear time domain nearshore models. A moving shoreline essentially means the computational domain is changing with the solution of the flow. The problem is solved in two steps. The first is to establish an equation that determines the motion of the shoreline based on the local momentum balance. The second is to develop and implement into a shoreline model the capability of accommodating a changing computational domain. The two models represent two different ways of addressing this step: one is to track the position of the shoreline in a fixed grid by establishing a special shoreline point which generally is not a fixed grid point. The second is by a coordinate transformation that maps the changing domain onto a fixed domain and solves the basic equations in the mapped domain. The two shoreline conditions are tested against three known solution for nonlinear shoreline motion. Two are the 1-D solutions to the nonlinear shallow water (NSW) equations by Carrier and Greenspan [J. Fluid Mech. 4 (1958) 97], one representing the response to a transient change in the offshore water level, the other the motion due to a periodic standing wave, both on slopes steep enough to allow full reflection. The third is the 2-D horizontal (2DH) computational solution by Zelt [Coast. Eng. 15 (1991) 205] for the run-up of a solitary wave on a cusped beach. In all cases, both models are shown to behave well and give high accuracy results for suitably chosen grid and time spacings.

Keywords: Shoreline condition; Numerical modeling; Fixed grid; Domain mapping

1. Introduction

One of the problems faced when modeling nearshore flows is to establish an appropriate representation at the shoreward boundary of the domain. Near the shoreline, flow properties change rapidly with the cross-shore position. A significant amount of sediment transport also occurs in the neighborhood of the shoreline. In order to be able to predict these processes and the flow in the swash region, an accurate and efficient model for the treatment of the shoreline is required.

Depth integration, which is used in many nearshore models to reduce complete three-dimensional (3-D) governing equations to 2-D horizontal (2DH), provides excellent results in the nearshore. However, as the water depth goes to zero at the shoreline, the convenient description based on volume fluxes rather than velocities degenerates to zero at the shoreline. At finite depth, velocities can be calculated by dividing the fluxes by the water depth. This, however, cannot be done at the shoreline, and this results in the necessity

* Corresponding author. Tel.: +1-302-831-2442; fax: +1-302-831-1228.

E-mail address: ias@coastal.udel.edu (I.A. Svendsen).

0378-3839/$ - see front matter
doi:10.1016/S0378-3839(03)00050-4

to carefully consider the proper equation for the motion of the shoreline itself.

The nonzero particle velocity at the shoreline changes the shoreline position with time which results in a time-varying fluid domain in the numerical computations.

Therefore, the problem at hand can essentially be divided into two parts: first, to develop a description for the velocity of the shoreline and thus the changes in the shoreline position with time, and second, to devise a method to incorporate a time-varying model domain in the numerical scheme.

The simplest boundary condition that can be applied at the shoreward boundary of a model domain is a wall boundary condition at the initial shoreline. Under this condition, the shoreline does not move with time and the fluxes at the initial shoreline are always zero. As shown by Lynch and Gray (1980), this type of shoreline boundary condition does not affect the results even a moderate distance from the boundary very much, but near the boundary, it may result in significant errors.

In the past, the time-varying fluid domain has been modeled in Eulerian schemes essentially using either a wet–dry interface for the shoreline with fixed grids or a coordinate transformation, where the instantaneous model domain is transformed onto a fixed, evenly spaced, rectangular computational grid.

Due to its conceptual simplicity, many numerical models use fixed grids with a wet–dry interface to treat the moving shoreline. Reid and Bodine (1968) were among the first to use this type of model at the shoreline. This scheme was used in a storm surge model, where the bottom elevation was assumed to be constant over each grid interval. This results in a stairstep-like approximation of the actual topography. The flux through the last wet grid point to the first dry grid point was given by an empirical relation that was a function of the height of the water column in the wet grid above the land elevation in the dry grid. Hibberd and Peregrine (1979), in another fixed grid method, used linear extrapolation to describe the run-up of a uniform bore on a plane-sloping beach. The first dry grid point was included in the computational domain if the water depth at that point was greater than a threshold value. Similarly, during run-down, the last wet point was excluded from the computational domain when the water depth there goes below a threshold value. Kobayashi et al. (1987), Militello (1998), Liu et al. (1995) and Balzano (1998) are some of the other implementations of a fixed grid method for treatment of shoreline. These methods had slightly different criteria for declaration when a grid point becomes wet or dry. They also differed in the way to calculate the volume of water left in a grid interval after it was declared dry. However, all the methods discussed above determine the position of the shoreline as one of the fixed grid points, which means the shoreline is moved one or more Δx at a time. This makes the wet–dry methods more prone to instabilities.

Sielecki and Wurtele (1970) and VanDongeren and Svendsen (1997) introduced ways to determine the actual shoreline position. In a fixed grid, the shoreline position will generally fall between two grid points, the last wet and the first dry point in the shoreward direction. Sielecki and Wurtele (1970) determines the shoreline position between the last wet and the first dry grid points by using a linear extrapolation of the surface elevation and velocity to the shoreline from the neighboring wet points. This approach has recently been explored further by Lynett et al. (2002) who determined (imaginary) values of both the surface elevation and the fluid velocity at the first two dry points by linear extrapolation from the two last wet points. Those imaginary values were then used in their fourth-order space derivatives needed in a predictor–corrector method similar to the scheme used in the present paper to solve the equations. VanDongeren and Svendsen (1997) determined by extrapolation the volume of water stored past the last wet point and assumed a triangular shape of that to estimate the actual shoreline position. When the distance of the shoreline from the last wet point becomes more than a grid spacing, the first dry grid point was declared wet and was included in the calculations at the next time steps. Similarly, when this distance becomes less than zero, the last wet point is excluded from the computational domain at the next time steps. However, as also discussed by Lynett et al. (2002), these methods based on extrapolation are very sensitive to numerical noise and frequently become unstable unless proper filtering is applied.

In the fixed grid method described here, the position of the shoreline is determined as a special point positioned between the last wet and the first dry grid point. This is done by solving the momentum equation for a fluid particle at the shoreline.

The other category of methods for treatment of the moving shoreline, which have been described in the literature, is the use of a coordinate transformation. In this method, the real, time-varying physical domain is transformed onto a time-invariant, computational domain. As the moving shoreline changes the cross-shore length of the domain, most of the coordinate transformation schemes used to model this change the grid spacing only in the cross-shore direction.

An early example of coordinate transformation methods (or domain mapping) is Joseph (1973). The simplest type of coordinate transformation scheme to achieve this goal was used by Johns (1982) where a linear mapping of the time-varying real domain x=[0, $L(t)$] is transformed onto a fixed computational domain X=[0, 1] using the transformation $X = x/L(t)$. Johns et al. (1982) describe another similar approach of coordinate transformation which was used for the modeling of storm surges on the east coast of India. Shi and Sun (1995) describe a coordinate transformation method that takes into account the time-varying shoreline in their finite difference model for storm surge in the generalized curvilinear coordinate. In these methods, the horizontal coordinates get transformed and the velocities also get modified so that the modified velocity in the transformed plane is zero.

Jamet and Bonnerot (1975), Lynch and Gray (1980) and Gopalakrishnan and Tung (1983) describe a few examples of implementation of a transformation method in finite element models. Jamet and Bonnerot (1975) and Lynch and Gray (1980) used continuously deforming finite elements where the last element followed the fluid boundary. Gopalakrishnan and Tung (1983) used Lagrangian acceleration to find the motion of the shoreline and a variable element length, which splits into two parts when this length becomes larger than 1.2 times the initial element length.

Özkan Haller and Kirby (1997) used a shoreline transformation technique to take into account the moving shoreline using a Chebyshev collocation method to calculate spatial derivatives in the cross-shore direction. The coordinate transformation was done in two steps that provided smaller grid spacings in the region closest to the shoreline where a higher resolution is required than the rest of the domain. However, this effect is included in the second transformation and hence cannot be used with other numerical schemes.

With the use of Lagrangian description, moving boundaries can be treated efficiently. Some examples of this are presented in Pedersen and Gjevik (1983), Zelt and Raichlen (1990) and Zelt (1991).

Brocchini and Peregrine (1996) suggest different ways of analyzing the mean shoreline for wave-averaged models and outline a method of treatment of the moving shoreline for such models as the lower edge of the swash by using the integral flow properties of the swash zone. The work by DeSilva et al. (1996), which includes the effect of surface tension, is also mentioned.

The approach adopted in the present work is to derive the equations for shoreline motion, and then any method (transformation or fixed grid) can be used to model a time-varying fluid domain. An example of fixed grid method and another example of coordinate transformation method are described.

The paper is structured as follows. In Section 2, the governing equations and its solution method are described. Section 3 describes the different methods used for inclusion of a time-varying fluid domain, i.e. the fixed grid method and the coordinate transformation method. Section 4 contains comparison of the results between the model computations with the shoreline boundary condition implemented using both these methods and the analytical results for 1-D cases as given by Carrier and Greenspan (1958) and the numerical results for 2-D cases given by Zelt (1986) and Özkan Haller and Kirby (1997). Finally, discussions and conclusion are described in Section 5.

2. Governing equations and solution scheme

2.1. Governing equations in the interior domain

Near the shoreline, the nonlinear motion with sufficiently large horizontal scale can be described by the nonlinear shallow water (NSW) equations. In cases where the motion is generated by local forcing, such as short-wave-generated infragravity waves, the forcing makes the NSW equations inhomogeneous. An example is the equations used in, e.g., the SHORECIRC (SC) nearshore circulation model. The model equations are the continuity and momentum equations which, for the general case of depth-varying currents, are given by, e.g., VanDongeren and Svendsen (1997), Sancho and Svendsen (1997) and Haas and Svendsen (2000).

These equations can be written as inhomogeneous NSW equations by placing all the contributions to changes in the NSW operator on the right-hand side of the equations. The result is

$$\frac{\partial \zeta}{\partial t}+\frac{\partial Q_\alpha}{\partial x_\alpha}=R_1 \tag{1}$$

$$\frac{\partial Q_\beta}{\partial t}+\frac{\partial}{\partial x_\alpha}\left(\frac{Q_\alpha Q_\beta}{h}\right)+g(h_0+\zeta)\frac{\partial \zeta}{\partial x_\beta}=R_{2\beta} \tag{2}$$

where g is the acceleration of gravity. Here, R_1 and $R_{2\beta}$ include the short-wave forcing (radiation stress and short-wave volume flux), the dispersive lateral mixing, the surface and bottom shear stress and the turbulent stress terms that are part of the mass and the momentum equations, respectively. In the following, these terms are referred to as the source terms. In a similar way, in the case of a Boussinesq approximation, the source terms on the RHS would represent the nonlinear-dispersive terms.

Fig. 1 shows the definitions of the geometrical variables used.

2.2. Equations for the shoreline motion

The depth-averaged Eqs. (1) and (2) give the fluid flow in terms of the volume fluxes and the surface elevation. At the shoreline, where the water depth goes to zero, the volume fluxes also become zero, but the velocity of the fluid particles, which are calculated by dividing the fluxes by the water depth, may not become zero. This velocity cannot be calculated by using the depth-integrated equations of motion as the water depth is zero there. Here, we will derive the equations to calculate the velocities at the shoreline and the shoreline position, once the velocities are known.

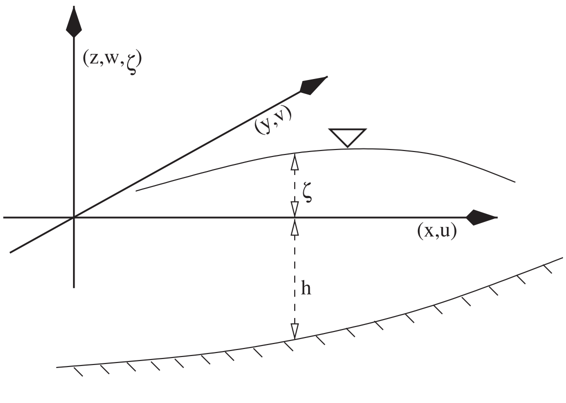

Fig. 1. Definition sketch.

The source terms in the governing equations do not change the principal nature of the problem at the shoreline, so for simplicity, we are, in the following, focusing on the homogeneous version of the equations.

2.2.1. Velocity of the shoreline

The x component of the homogeneous version of Eq. (2) can be written as

$$\frac{\partial Q_x}{\partial t}+\frac{\partial}{\partial x}\left(\frac{Q_x^2}{h}\right)+\frac{\partial}{\partial y}\left(\frac{Q_x Q_y}{h}\right)+gh\frac{\partial \zeta}{\partial x}=0 \tag{3}$$

On substituting $Q_x=uh$ and $Q_y=vh$ in Eq. (3) and using the continuity equation, we get

$$h\frac{\partial u}{\partial t}+hu\frac{\partial u}{\partial x}+hv\frac{\partial u}{\partial y}+gh\frac{\partial \zeta}{\partial x}=0 \tag{4}$$

or, for any arbitrarily small $h>0$,

$$\frac{\partial u}{\partial t}+u\frac{\partial u}{\partial x}+v\frac{\partial u}{\partial y}=-g\frac{\partial \zeta}{\partial x} \tag{5}$$

If we assume that a particle at the shoreline will remain at the shoreline, the LHS of Eq. (5) will also represent the acceleration of the shoreline itself in the x direction. Hence, we have the x component of the velocity u^s of the shoreline point (denoted by superscript s) given by

$$\frac{\mathrm{d}u^s}{\mathrm{d}t}=-g\frac{\partial \zeta^s}{\partial x} \tag{6}$$

On extending this to the 2DH case, u^s and y component v^s of the velocity of the shoreline can be determined from the equations

$$\left.\frac{\mathrm{d}u^s(y,t)}{\mathrm{d}t}\right|_y=-g\frac{\partial \zeta^s}{\partial x} \tag{7}$$

and

$$\left.\frac{\mathrm{d}v^{s}(y,t)}{\mathrm{d}t}\right|_{y} = -g\frac{\partial \zeta^{s}}{\partial y} \tag{8}$$

Here, u^s and v^s are calculated along a line of constant y so that the shoreline motion can be calculated by Eq. (12). Hence, Eqs. (7) and (8) represent the general 2DH equations which will be used in the following to determine by integration in time the horizontal velocities of the shoreline points with coordinates (x^s, y^s).

2.2.2. Position of the shoreline

The kinematic condition at the shoreline states that the fluid particles at the shoreline remain at the shoreline. This provides us with an equation to calculate the time variation of the shoreline position when the particle velocity at the shoreline is known. If $x = \xi(y,t)$ is the x coordinate for the shoreline as shown in Fig. 2, then the shoreline is given by

$$S = x - \xi = 0 \tag{9}$$

We therefore have the kinematic condition,

$$\frac{\mathrm{D}S}{\mathrm{D}t} = 0 \Rightarrow \frac{\mathrm{D}(x-\xi)}{\mathrm{D}t} = 0 \tag{10}$$

where

$$\frac{\mathrm{D}}{\mathrm{D}t} = \frac{\partial}{\partial t} + u^{s}\frac{\partial}{\partial x} + v^{s}\frac{\partial}{\partial y} \tag{11}$$

is the derivative following the shoreline. On expanding the derivatives, we get

$$\frac{\partial \xi}{\partial t} = u^{s} - v^{s}\frac{\partial \xi}{\partial y} \tag{12}$$

The assumption here is that the shoreline position is a single-valued, continuous function of the longshore coordinate y at any time t.

The surface elevation ζ^s at the shoreline can be calculated when the horizontal shoreline position obtained by Eq. (12) and the bottom topography are known. This, in turn, can be used to calculate the surface gradient terms on the right-hand side of Eqs. (7) and (8).

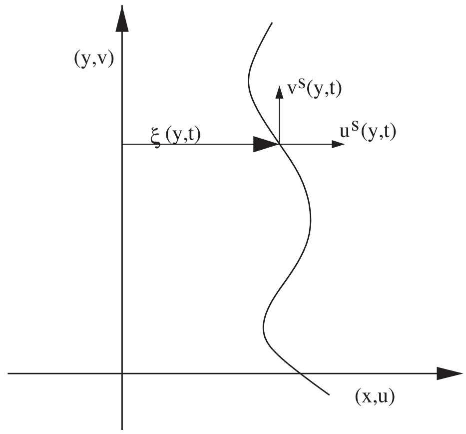

Fig. 2. Definition sketch for the shoreline position.

3. Methods to compute a time-dependent fluid domain

The time-varying shoreline position computed by Eq. (12) results in a time-dependent boundary value problem that is to be modeled in a numerical simulation. Two different methods are described in the following for the treatment of this problem. In the first method, the shoreline position is treated as a special point between equally spaced grid points, whereas in the second method, the last grid point always represents the shoreline and the grid spacing near the shoreline changes as the shoreline moves.

3.1. Fixed grid method

In this approach to adopt a time-varying model domain, the computational domain is discretized on a fixed grid and the shoreline is defined as the point separating wet and dry regions, which need not be a grid point. In order to do this, the last wet and the first dry grid points are identified and the shoreline point is treated as a special point between these grid points. When the shoreline passes a dry grid point while moving in the shoreward direction, that grid point is included in the active calculation zone, which is the wet region of the domain, at the following time steps of the computation. Similarly, when a wet grid point is passed in the seaward motion of the shoreline, it is excluded from the active calculations in the following time steps.

In the past, most of the implementations using fixed grid points with wet–dry interface do not resolve the shoreline position between the last wet and the first dry point. Many such examples were discussed in Section 1. Sielecki and Wurtele (1970) and VanDongeren and Svendsen (1997) give a few examples where the shoreline position between the last wet and the first dry grid points was determined, though they use extrapolation schemes to do this. In the method used by VanDongeren and Svendsen (1997), the shoreline position between the last wet and the first dry point was determined along with the surface elevation at the last wet point. This was done by calculating the volume of water stored past the last wet point and assuming a linear variation of the surface elevation from the last wet point to the shoreline point. The volume flux at the last wet point was also obtained by interpolation.

In the method described here, the velocities of the fluid particles at the shoreline are obtained first. The shoreline position is then calculated by using these velocities. The actual shoreline position is calculated at each time step, and thus the position of the shoreline between the last wet and the first dry grid points is known.

3.1.1. Spatial derivatives near the shoreline

Since the distance between the last wet point and the shoreline point is not the same as the constant grid spacing in the rest of the domain, and this spacing also changes with time, the finite difference formulation for spatial derivatives near the shoreline needs to be modified. This is done by using the Taylor series expansion and obtaining the spatial derivative formula for a nonconstant grid spacing near the shoreline.

The shoreline position is identified as x_s, the last wet grid position as x_0 and the second last wet grid position as x_1. The spacing between x_1 and x_0 is Δx which is the grid spacing in the rest of the domain. The spacing between x_0 and x_s changes with time. The ratio of this distance to the constant grid spacing in the rest of the domain Δx is denoted by s. A sketch of the domain near the shoreline is given in Fig. 3.

The derivatives of the variables at x_s and at the last wet grid point x_0 are determined in the following way.

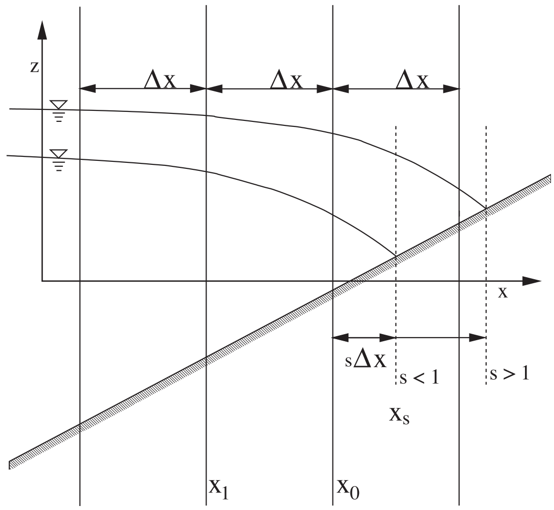

Fig. 3. Domain near the shoreline. x_s is the shoreline position. x_0 and x_1 are the last two wet points. Notice that during the motion of the shoreline, s>1 is used in some phases (see Section 3.1.2).

The Taylor series expansion of a function $f(x)$ about the last wet grid point x_0 is given by

$$f(x_s) = f(x_0 + s\Delta x) = f(x_0) + s\Delta x f'(x_0) + \frac{(s\Delta x)^2}{2!} f''(x_0) + O(\Delta x^3) \tag{13}$$

$$f(x_1) = f(x_0 - \Delta x) = f(x_0) - \Delta x f'(x_0) + \frac{(\Delta x)^2}{2!} f''(x_0) + O(\Delta x^3) \tag{14}$$

where the primes indicate derivatives in x. Multiplying Eq. (14) by $(s\Delta x)^2$ and subtracting from Eq. (13) eliminates $f''(x_0)$ and a relation for $f'(x_0)$ in terms of $f(x_0)$, $f(x_1)$ and $f(x_s)$ is obtained as

$$f'(x_0) = \frac{f(x_s) + (s^2 - 1) f(x_0) - s^2 f(x_1)}{s(s+1)\Delta x} \tag{15}$$

Similarly, $f'(x_s)$ can be obtained as

$$f'(x_s) = \frac{(1+2s) f(x_s) - (1+s)^2 f(x_0) + s^2 f(x_1)}{s(s+1)\Delta x} \tag{16}$$

3.1.2. Addition and deletion of a grid point

In this method, the active calculation zone is the wet region where the fluxes and the surface elevations are calculated by solving the continuity and the momentum equations. The second part of the computational domain is the dry region shoreward of x_s. This region is sufficiently described by

$$h_0 + \zeta = 0 \quad \text{or} \quad \zeta = -h_0 \tag{17}$$

$$Q_x = 0 \tag{18}$$

$$Q_y = 0 \tag{19}$$

At the shoreline, the velocity components are calculated by integration of Eqs. (7) and (8), and then the horizontal position of the shoreline point is calculated by time integration of Eq. (12). The surface elevation at the shoreline point is then calculated by

$$\zeta_s = -(h_0)_s \tag{20}$$

and the volume fluxes Q_α there are zero.

In the cases where the bottom topography is given analytically, h_{0s} can be calculated directly when the shoreline position is known. In other cases, it has to be obtained by interpolation between the undisturbed water depths at the regularly spaced grid points near the shoreline.

The ratio of the distance of the shoreline position from the last wet grid to the constant grid spacing Δx, s, appears in the denominator of Eqs. (15) and (16), so $s=0$ must be avoided during the motion of the shoreline. Therefore, it is necessary to choose a small, fixed minimum value for $s=s_{\min}$. During run-down, if $s<s_{\min}$, it is assumed that the last wet grid point (x_0) has become dry, so that the grid point is removed from the active calculation zone and the value of s is increased by 1, so that we have $s\Delta x>\Delta x$.

Similarly, during run-up, the first dry grid point going shoreward is not included in the active calculation region until the value of s becomes larger than $1+s_{\min}$. When $s>1+s_{\min}$, the first dry grid point is declared to become a wet point and is included in the active calculation zone. The value of s is then decreased by 1. In most of the simulations described later on, we will use $s_{\min}=0.5$.

3.1.3. Fixed grids for 2DH cases

In the 2DH case, some extra care is needed in order to apply the boundary condition at the shoreline using a fixed grid and a wet–dry interface. The difference from the 1DH case is that now, the last wet points and the shoreline points are functions of longshore position.

The model domain is divided in this case into three regions. In the first region, all the grid points in the longshore direction are wet. In the second region, some of the grid points in the longshore direction are wet, and in the third region, none of the grid points in the longshore direction are wet. Fig. 4 shows these three regions for a typical model domain. Extending the 1DH formulation to 2DH is straightforward in the regions one and three since all the grid are either wet or dry.

In the region II, the x derivatives near the shoreline can be calculated by Eqs. (15) and (16) as before. To obtain the y derivatives in this region, a fourth-order central difference formula has been applied if there are two wet points on both sides of a wet point along the y direction; otherwise, a second-order finite difference formula has been applied.

The y component of the velocity also needs to be calculated using Eq. (8) before Eq. (12) can be used for calculation of the shoreline position. Thus, the y derivatives are to be calculated at and near the shoreline, and filters are applied in the longshore direction y also. The difficulty in the calculation of y gradients at the shoreline is due to the fact that at an arbitrary shoreline position, there may not be grid

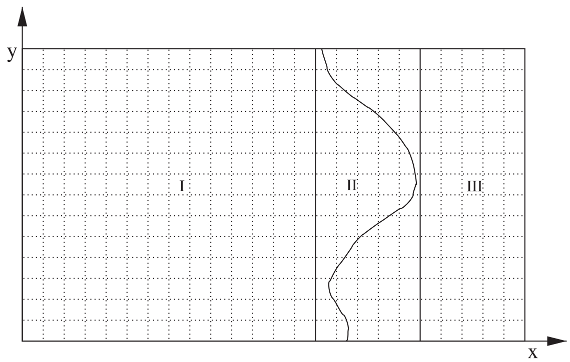

Fig. 4. Three regions in 2DH case with fixed grid and wet–dry interface. Region I has all the grid points wet, region III has all the grid points dry and region II has some grid points which are wet.

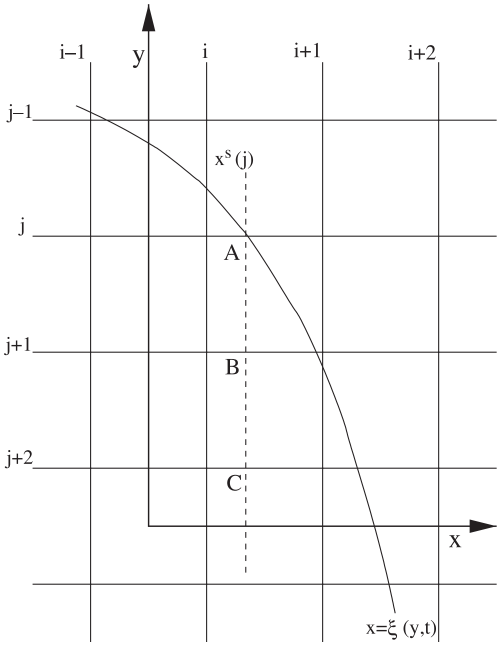

Fig. 5. A typical situation encountered in calculation of the y derivative at the shoreline. (– – –) marks the shoreline position at the jth grid point in the y direction.

points in the longshore direction, as $s(y)$, in general, can have different values at different longshore locations. It can be seen in Fig. 5 that in order to calculate y derivatives at a shoreline point A, the variables at the points B and C should be known. However, as B and C are neither regular grid points nor shoreline points, the values of the variables at these points are obtained by extrapolation along the $j+1$ and $j+2$ lines (Fig. 5).

Thus, we use

$$f(B) = a\{s(j)\}^2 + bs(j) + c \tag{21}$$

with $s(j)=(x^s(j) - x(i))/\Delta x$, which was used to calculate the value of f at point B. Here,

$$a = \frac{1}{2}\{f(i,j+1) - 2f(i-1,j+1) + f(i-2,j+1)\} \tag{22}$$

$$b = \frac{1}{2}\{3f(i,j+1) - 4f(i-1,j+1) + f(i-2,j+1)\} \tag{23}$$

and

$$c = f(i,j+1) \tag{24}$$

Similarly, $j+1$ was replaced by $j+2$ to calculate the variables at the point C. The second-order forward difference equation,

$$\left.\frac{\partial f}{\partial y}\right|_A = \frac{1}{2\Delta y}\{-3f(A) + 4f(B) - f(C)\} \tag{25}$$

was then used to calculate the derivative at the point A as the distances between A and B and B and C are same and equal to Δy. In cases where too few points are available in the y direction at a given $x(j)$ level, symmetry is assumed resulting in no longshore variation, and the y derivatives are set to zero.

Similar formulas were used in cases where the wet point in the vicinity of the shoreline is on the left side of the shoreline point. In this case, backward difference equations were used instead of Eq. (25).

3.2. The grid transformation method

Another method of implementation of a time-varying domain in a numerical model which will be described here uses a coordinate transformation such that the instantaneous physical domain, which expands and contracts as the shoreline is moving, gets mapped onto a fixed domain in the transformed coordinate system. Near the shoreline, velocities and surface elevations often have large gradients.

In selecting a coordinate transformation scheme, which has a primary aim of mapping the irregular and time-varying shoreline onto a fixed grid in the computational domain, constraints can be prescribed here so that a smaller grid spacing near the shoreline than the rest of the domain can be obtained. This transformation is expected to result in a computational grid, which has evenly spaced grid points in the computational domain, and which corresponds to a grid with varying spacing in the physical domain at any given time.

The governing equations described earlier are derived for rectangular Cartesian coordinates. On introduction of this coordinate transformation, the governing equations need to be modified to take into account the grid spacing variation and distortion.

3.2.1. Model domain definitions

The actual physical domain (x, y, t) extends from $x=0$ to $x=L+\xi$ and $y=0$ to $y=Y$. Here, $\xi(y, t)$ is the

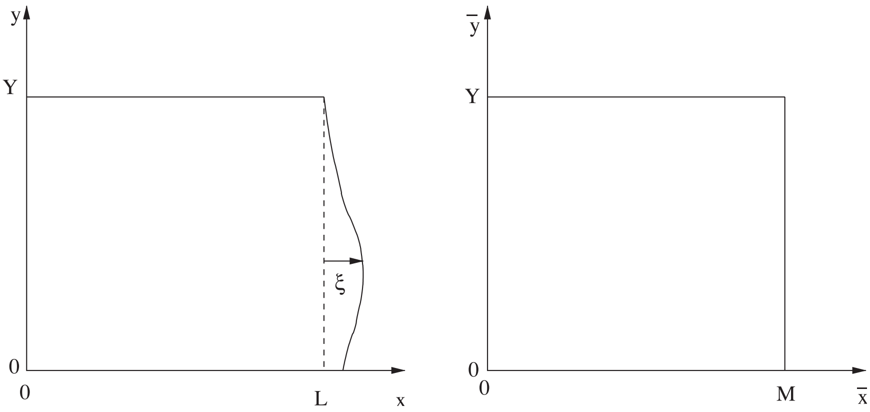

Fig. 6. Sketches of the real (on the left) and the transformed (on the right) model domains.

shoreline position measured from a reference level $x = L$ (see Fig. 6). In most cases, the initial shoreline position can be taken to be this reference level. The physical domain is transformed onto a computational domain ($\bar{x}$, $\bar{y}$, $\bar{t}$) by the transformation equations,

$$x = g(\bar{x}) + \xi(y,t)f(\bar{x}) \tag{26}$$

$$y = \bar{y} \tag{27}$$

$$t = \bar{t} \tag{28}$$

The computational domain extends from $\bar{x} = 0$ to $\bar{x} = M$ and $\bar{y} = 0$ to $\bar{y} = Y$. A sketch of the real and the computational domains are shown in Fig. 6.

3.2.2. Conditions on the transformation functions

The function $f(\bar{x})$ is selected such that the transformation maps the irregular shoreline onto a fixed, straight line in the computational domain, whereas the function $g(\bar{x})$ is selected such that this transformation yields smaller grid spacing near the shoreline than that offshore.

Since the offshore boundary of the real and the computational domains should be at the same location,

$$\bar{x} = 0 \Rightarrow x = 0 \tag{29}$$

we must have

$$f(0) = 0; \quad g(0) = 0 \tag{30}$$

Similarly, the shoreline in both the domains must coincide, so,

$$\bar{x} = M \Rightarrow x = L + \xi \tag{31}$$

Hence, f and g must satisfy

$$f(M) = 1; \quad g(M) = L \tag{32}$$

Without loss of generality, we can assume that $L = M$ as it does simplify the calculations later on. Now, $\Delta x/\Delta\bar{x} = 1$ implies an equal grid spacing in both the domains.

The grid size distribution in the cross-shore direction is given by

$$\frac{\Delta x}{\Delta\bar{x}} = g'(\bar{x}) + \xi(y,t)f'(\bar{x}) \tag{33}$$

The condition that the grid spacing near the shoreline should be smaller than that offshore is expressed mathematically by

$$0 < \left[\left(\frac{\Delta x}{\Delta\bar{x}}\right)_{\bar{x}=M} = g'(M) + \xi(y,t)f'(M)\right] < 1 \tag{34}$$

$\Delta x/\Delta\bar{x} = 0$ would imply that two points in the computational domain correspond to one point in the physical domain. Since the inverse of the transform would not be unique in this case, it must be avoided in the transformation used here.

3.2.3. Selection of the transformation functions

Any function which satisfies the conditions described in Section 3.2.2 can be used in the transformation equations. The conditions on the function $f(\bar{x})$ state that it goes from 1 to 0 as $\bar{x}$ goes from the shoreline $\bar{x}=M$ to the offshore boundary of the model domain $\bar{x}=0$.

Different analytical functions which have a variation with $\bar{x}$ similar to the one required by the conditions on $f(\bar{x})$ were tried and

$$f(\bar{x}) = (\mathrm{e}^{-\kappa(M-\bar{x})} - \mathrm{e}^{-\kappa M})/(1-\mathrm{e}^{-\kappa M}) \tag{35}$$

was used in most of the simulations described here.

The purpose of the function $g(\bar{x})$ is to ensure a certain variation of $\Delta x/\Delta\bar{x}$. Since the variation of $\Delta x/\Delta\bar{x}$ is directly related to the derivative $g'(\bar{x})$ of $g(x)$, it is easier to obtain the desired variation of $\Delta x/\Delta\bar{x}$ if we select $g'(\bar{x})$ directly. Thus, we require

$$g'(M) < 1 \tag{36}$$

and

$$\int_0^M g'(\omega)\mathrm{d}\omega = M \tag{37}$$

and then calculate $g(\bar{x})$ by

$$g(\bar{x}) = \int_0^{\bar{x}} g'(\omega)\mathrm{d}\omega \tag{38}$$

For any $f'(M)\neq 0$, the grid size distribution $\Delta x/\Delta\bar{x}$ will be greater or smaller there than $g'(M)$ depending on the sign of ξ. If $g'(M)=0.5$, then for any given $f'(M)$, $(\Delta x/\Delta\bar{x})_{\bar{x}=M}$ can accommodate maximum variation of ξ about $\xi=0$. In most of the simulations described afterward, $g'(M)=0.5$ will be used. Fig. 7 shows the effect of different ξ on $\Delta x/\Delta\bar{x}$ for one particular choice of $f(\bar{x})$ and $g(\bar{x})$. It can be seen that the grid spacing near the shoreline ($\bar{x}=M$) is smaller than that offshore ($\bar{x}=0$) but it changes with ξ. During the highest run-up ($\xi=3$ in the example), the grid is stretched and $\Delta x/\Delta\bar{x}$ increases somewhat toward the shoreline. When the shoreline is in the lowest position of run-down ($\xi=-3$), the resolution at the shoreline is very high with $\Delta x/\Delta\bar{x}=0.2$ only. Thus, a very high resolution is obtained during phase of the run-down that is also the phase with the strongest spatial variations and potential wave breaking.

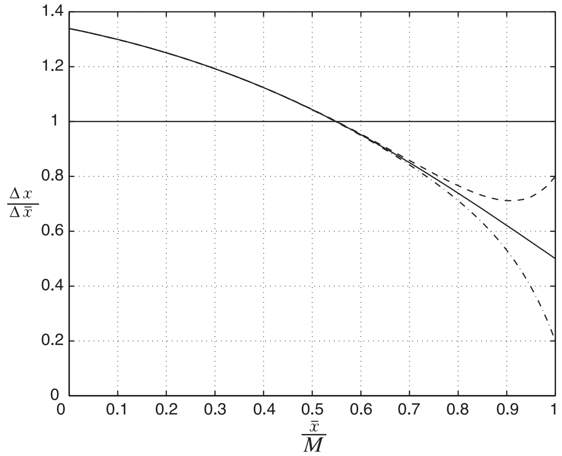

Fig. 7. $\Delta x/\Delta\bar{x}$ for different ξ with $f(\bar{x})=(\mathrm{e}^{-\kappa(M-\bar{x})}-\mathrm{e}^{-\kappa M})/(1-\mathrm{e}^{-\kappa M})$ and $g(\bar{x})$ given by Eq. (42). (——) $\xi=0$; (– – –) $\xi=3$; (- - - - -) $\xi=-3.0$, for $a=0.01015$ and $\kappa=0.1$.

We have only two required conditions on the function $g(\bar{x})$ and one of them has been used to determine the value of $g'(M)$. Therefore, only one condition is left on $g(\bar{x})$. It can be uniquely determined if it has only one free parameter. If, for example, a polynomial of $\bar{x}$ is assumed for $g'(\bar{x})$, only a linear function can be determined uniquely and that is

$$g'(\bar{x}) = 0.5 + \frac{M-\bar{x}}{M} \tag{39}$$

For a second-degree polynomial, a family of functions for $g'(\bar{x})$ given by

$$g'(\bar{x}) = 0.5 + a(M-\bar{x}) + b(M-\bar{x})^2 \tag{40}$$

is obtained. Here, a and b must satisfy the relation

$$3aM + 2bM^2 = 3 \tag{41}$$

which is obtained by substituting Eq. (40) into condition (37).

Different functions have been tested for $g'(\bar{x})$. Fig. 8 shows some possible choices for $g(\bar{x})$. For most of the model simulations described afterward, we have used

$$g'(\bar{x}) = 0.5 + \tanh\{a(M-\bar{x})\} \tag{42}$$

Here, a is calculated so that $g(0)=0$ is satisfied. It can be seen in Fig. 8 that the region where $g'(\bar{x})<1$ is

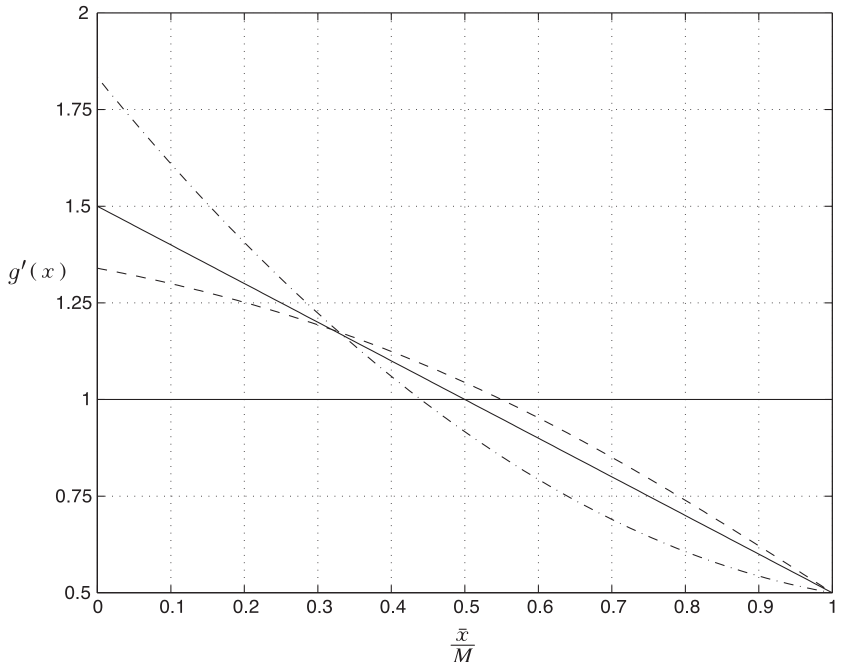

Fig. 8. Some possible choices for $g'(\bar{x})$. (——) represents Eq. (39); (– – –) represents Eq. (42); and (– - - - –) is $g'(\bar{x})$ given by Eq. (40), with $a = 1/3M$ and $b = 1/M^2$ for $M = 20$ m.

smaller for $g'(\bar{x})$ given by Eq. (42). Therefore, the region of $\Delta x/\Delta \bar{x} < 1$ is concentrated near the shoreline where a high resolution is required.

3.2.4. Modification of the governing equations due to the transformation

In order to be able to perform calculations in the ($\bar{x}$, $\bar{y}$, $\bar{t}$) coordinate system, the derivatives with respect to x, y and t in the continuity and the momentum equations need to be changed to the derivatives with respect to $\bar{x}$, $\bar{y}$ and $\bar{t}$. These changes can be obtained by implicit differentiation.

For the simplified form of the transformation in the x direction only used here, we get

$$\frac{\partial}{\partial x} = \frac{\partial}{\partial \bar{x}} \frac{\partial \bar{x}}{\partial x} \tag{43}$$

$$\frac{\partial}{\partial y} = \frac{\partial}{\partial \bar{y}} + \frac{\partial}{\partial \bar{x}} \frac{\partial \bar{x}}{\partial y} \tag{44}$$

$$\frac{\partial}{\partial t} = \frac{\partial}{\partial \bar{t}} + \frac{\partial}{\partial \bar{x}} \frac{\partial \bar{x}}{\partial t} \tag{45}$$

By differentiating the transformation equation (26) with respect to x, y and t and rearranging, we then get

$$\frac{\partial \bar{x}}{\partial x} = \frac{1}{g'(\bar{x}) + \xi(y,t)f'(\bar{x})} \tag{46}$$

$$\frac{\partial \bar{x}}{\partial y} = -\left\{\frac{1}{g'(\bar{x}) + \xi(y,t)f'(\bar{x})}\right\} \frac{\partial \xi(y,t)}{\partial y} f(\bar{x}) \tag{47}$$

$$\frac{\partial \bar{x}}{\partial t} = -\left\{\frac{1}{g'(\bar{x}) + \xi(y,t)f'(\bar{x})}\right\} \frac{\partial \xi(y,t)}{\partial t} f(\bar{x}) \tag{48}$$

respectively. Substitution from Eqs. (46)–(48) into Eqs. (44) and (45) results in

$$\frac{\partial}{\partial y} = \frac{\partial}{\partial \bar{y}} - \frac{\partial}{\partial \bar{x}} \frac{\partial \bar{x}}{\partial x} \frac{\partial \xi}{\partial y} f(\bar{x}) \tag{49}$$

$$\frac{\partial}{\partial t} = \frac{\partial}{\partial \bar{t}} - \frac{\partial}{\partial \bar{x}} \frac{\partial \bar{x}}{\partial x} \frac{\partial \xi}{\partial t} f(\bar{x}) \tag{50}$$

On applying these modifications from Eqs. (43), (49) and (50) to the mass and the momentum equations, the governing equations are modified to the following form

$$\frac{\partial \zeta}{\partial \bar{t}} - \frac{\partial \zeta}{\partial \bar{x}}\frac{\partial \bar{x}}{\partial x}\frac{\partial \xi}{\partial t}f(\bar{x}) + \frac{\partial Q_x}{\partial \bar{x}}\frac{\partial \bar{x}}{\partial x} + \frac{\partial Q_y}{\partial \bar{y}} - \frac{\partial Q_y}{\partial \bar{x}}\frac{\partial \bar{x}}{\partial x}\frac{\partial \xi}{\partial y}f(\bar{x}) = 0 \tag{51}$$

$$\frac{\partial Q_x}{\partial \bar{t}} - \frac{\partial Q_x}{\partial \bar{x}}\frac{\partial \bar{x}}{\partial x}\frac{\partial \xi}{\partial t}f(\bar{x}) + \frac{\partial}{\partial \bar{x}}\left(\frac{Q_x^2}{h}\right)\frac{\partial \bar{x}}{\partial x} + \frac{\partial}{\partial \bar{y}}\left(\frac{Q_xQ_y}{h}\right) - \frac{\partial}{\partial \bar{x}}\left(\frac{Q_xQ_y}{h}\right)\frac{\partial \bar{x}}{\partial x}\frac{\partial \xi}{\partial y}f(\bar{x}) = -gh\frac{\partial \zeta}{\partial \bar{x}}\frac{\partial \bar{x}}{\partial x} \tag{52}$$

$$\frac{\partial Q_y}{\partial \bar{t}} - \frac{\partial Q_y}{\partial \bar{x}}\frac{\partial \bar{x}}{\partial x}\frac{\partial \xi}{\partial t}f(\bar{x}) + \frac{\partial}{\partial \bar{x}}\left(\frac{Q_xQ_y}{h}\right)\frac{\partial \bar{x}}{\partial x} + \frac{\partial}{\partial \bar{y}}\left(\frac{Q_x^2}{h}\right) - \frac{\partial}{\partial \bar{x}}\left(\frac{Q_x^2}{h}\right)\frac{\partial \bar{x}}{\partial x}\frac{\partial \xi}{\partial y}f(\bar{x}) = -gh\left[\frac{\partial \zeta}{\partial \bar{y}} - \frac{\partial \zeta}{\partial \bar{x}}\frac{\partial \bar{x}}{\partial x}\frac{\partial \xi}{\partial y}f(\bar{x})\right] \tag{53}$$

When the functions $f(\bar{x})$ and $g(\bar{x})$ are selected, the term $\partial\bar{x}/\partial x$ can be calculated by Eq. (46). Since ξ is known as a function of y at any time step n and also at the previous time steps $n-1$, $n-2$, etc., $\partial\xi/\partial y$ can be calculated at those time steps. As the components of the velocity of the shoreline are also known at that present time step n and previous time steps, $\partial\xi/\partial t$ can be calculated from Eq. (12), and then ξ at the next time step $n+1$ can be obtained by the time integration of this equation. Thus, all the terms in the modified governing equations (51)–(53) are known at a time step n and previous time steps, and a third-order ABM predictor–corrector scheme can be applied to calculate the volume fluxes and the surface elevation at the next time step for $\bar{x}=0$ to $\bar{x}<M$. At $\bar{x}=M$, a similar predictor–corrector scheme can also be used for Eqs. (7) and (8)) to obtain u^s and v^s, and then Eq. (12) is used to obtain the shoreline position ξ at the next time step.

4. Comparison with other solutions

Due to unavailability of detailed measurements of the shoreline motion, analytical solutions and other numerical solution for the simplified cases are used here for the comparison of the present model.

4.1. Analytical solutions in 1DH

4.1.1. Carrier and Greenspan's (CG58) transient case

The analytical solution of the nonlinear shallow water equations for plane-sloping beaches was obtained by Carrier and Greenspan (1958) (CG58) by using a series of transformations which finally express the NSW equations in terms of the variables σ^* and λ^* given by

$$\sigma^* = 4c^* \tag{54}$$

$$\lambda^* = 2(u^* + t^*) \tag{55}$$

where u is the horizontal velocity, t is the time and superscript * refers to a nondimensional form of the variables. c^* is the nondimensional phase speed which is equal to $\sqrt{d^*}$. For details, reference is made to CG58.

At the shoreline, the water depth $d^*=\zeta^*+h_0^*=0$, so $c^*=\sqrt{d^*}=0$, and thus with this transformation, $\sigma^*=0$ always represents the shoreline position.

The dependent variables x, ζ, t and u are obtained in terms of the independent variables σ and λ.

CG58 described some initial value problems and their analytical solution. In the transient case, the initial water surface elevation is assumed to have a depression near the shoreline and it is released from that state of rest at $t^*=0$. The situation is shown in Fig. 11 where the initial position is the curve except near the outer boundary. The surface elevation and corresponding x locations in the nondimensional form are given by

$$\zeta^* = \epsilon\left[1 - \frac{5}{2}\frac{a^3}{(a^2+\sigma^2)^{\frac{3}{2}}} + \frac{3}{2}\frac{a^5}{(a^2+\sigma^2)^{\frac{5}{2}}}\right] \tag{56}$$

$$x^* = -\frac{\sigma^2}{16} + \zeta^* \tag{57}$$

where ϵ is a small parameter, which characterizes the magnitude of the depression, and

$$a = 1.5(1 + 0.9\epsilon)^{\frac{1}{2}} \tag{58}$$

At $t^* = 0$, the solution assumes

$$u^* = 0 \tag{59}$$

The surface elevation becomes asymptotically equal to ϵ as x goes to infinity offshore and this is the maximum surface elevation. The minimum surface elevation is zero and it occurs at the shoreline at $t^* = 0$. Initial surface profile has a zero tangent at the shoreline and at $x^* = -1$, $\zeta^* = 0.9\epsilon$. For nonbreaking cases, the value of ϵ should be less than or equal to 0.23 as predicted by CG58.

The results are presented here for $\epsilon = 0.1$. The bottom slope α is taken to be 1/50 and the length scale l was selected to be 20 m.

Fig. 9 shows the nondimensional surface elevation as a function of the cross-shore distance x^* at time $t^* = 0$ to $t^* = 0.8$ in steps of $\Delta t^* = 0.05$ for the fixed grid method, and Fig. 10 shows the same for the coordinate transformation method.

Similarly, Figs. 11 and 12 show the time series of the nondimensional surface elevation at the shoreline for t^* up to 5 for the fixed grid and the coordinate transformation methods, respectively. As can be seen from these figures, the shoreline shoots past the maximum initial surface elevation ϵ and then slowly comes back to asymptotically approach ϵ as time t^* goes to infinity.

In all the figures above, the surface elevation has been scaled with the depression parameter ϵ.

We see that the results with both the methods of shoreline treatment are in excellent agreement with the analytical solutions.

To illustrate the numerical sensitivity of the fixed grid method, Fig. 13 shows computations with different values of Δx^*. The Courant number Cr is held constant corresponding to Δt^* values varying in consonance with Δx^*. We see that the numerical errors grow in a controlled way with increasing Δx^*.

For the coordinate transformation method, it was found that the somewhat larger $\Delta \bar{x}^* = 0.031$ gave

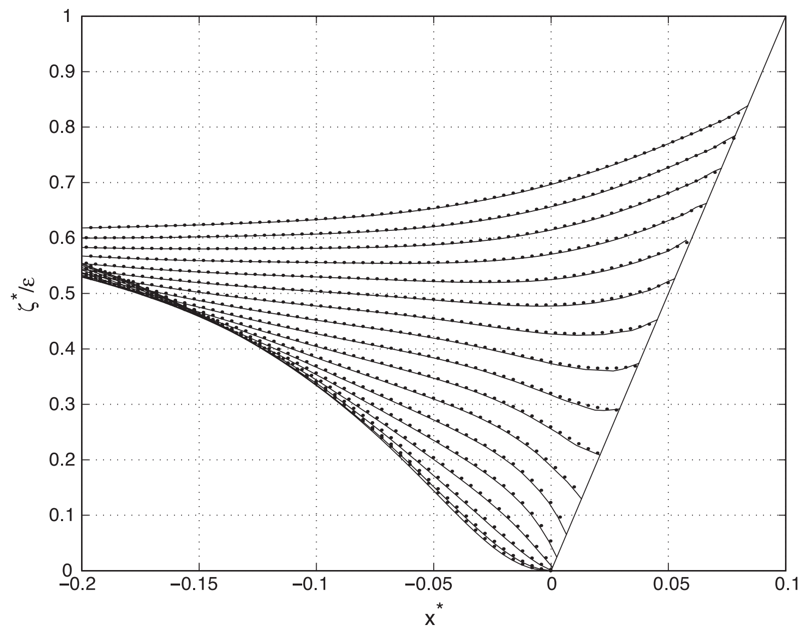

Fig. 9. CG58's transient case. Comparisons with a fixed grid of the surface elevation as a function of the cross-shore distance at different time steps. The analytical solution (▪ ▪ ▪); present model with fixed grid (——). The time $t^* = 0$ corresponds to the lowest position and the highest position of the shoreline shown corresponds to $t^* = 0.8$.

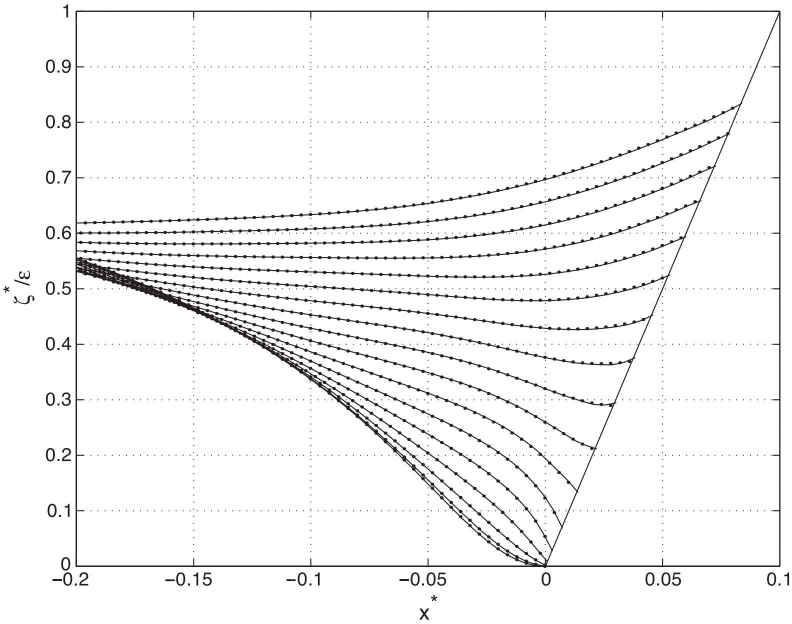

Fig. 10. CG58's transient solution: results with the coordinate transformation method for surface elevation as a function of the cross-shore distance at $t^*=0$ to $t^*=0.8$ at the steps of $\Delta t^*=0.05$. Analytical solution (▪ ▪ ▪); present model (——). $\Delta\bar{x}^*=0.007735$ and $\Delta t^*=0.025$ were used in the simulations.

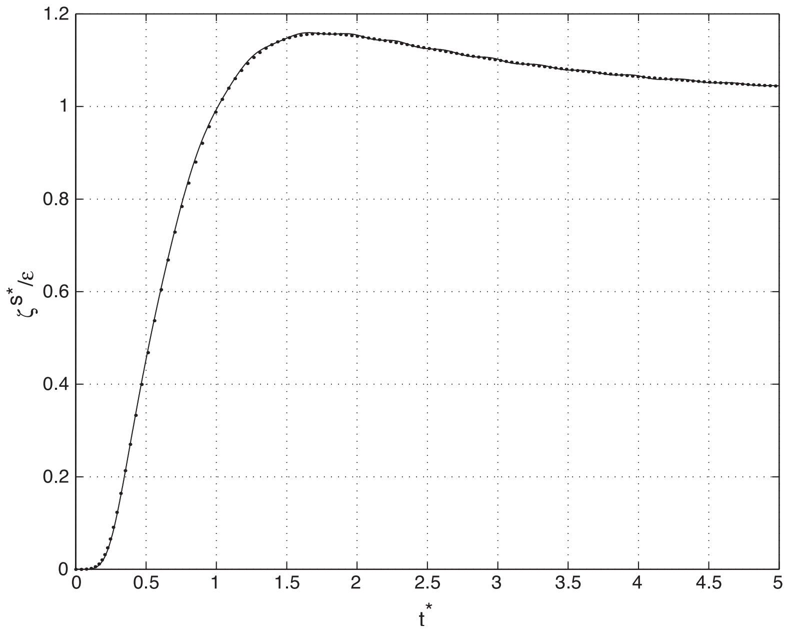

Fig. 11. CG58's transient case: fixed grid time series of the surface elevation at the shoreline. The analytical solution (▪ ▪ ▪); present model with fixed grid (——). The part up till $t^*=0.8$ corresponds to the time interval covered in Fig. 9.

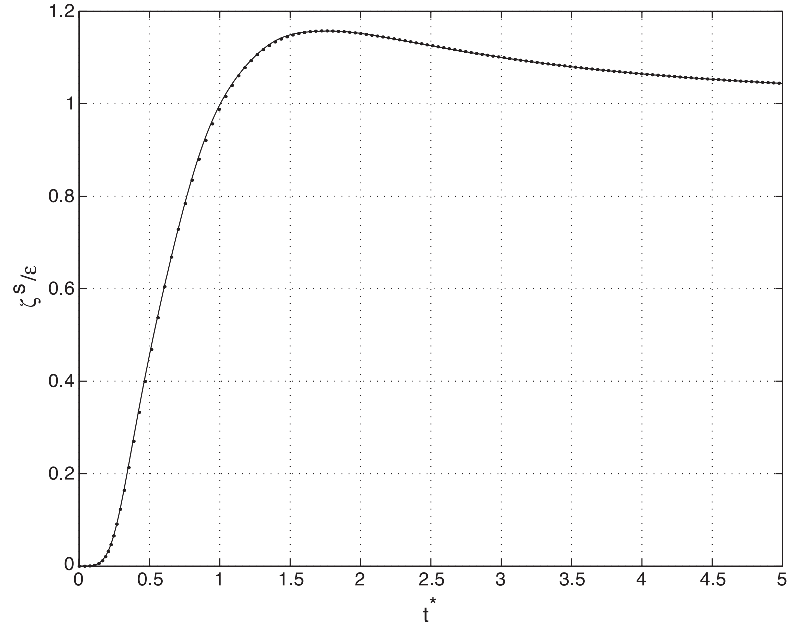

Fig. 12. CG58's transient solution: model results for the time series of the surface elevation at the shoreline with the coordinate transformation. Analytical solution (▪ ▪ ▪); present model (——). $\Delta\bar{x}^*=0.007735$ and $\Delta t^*=0.025$ were used in the simulations.

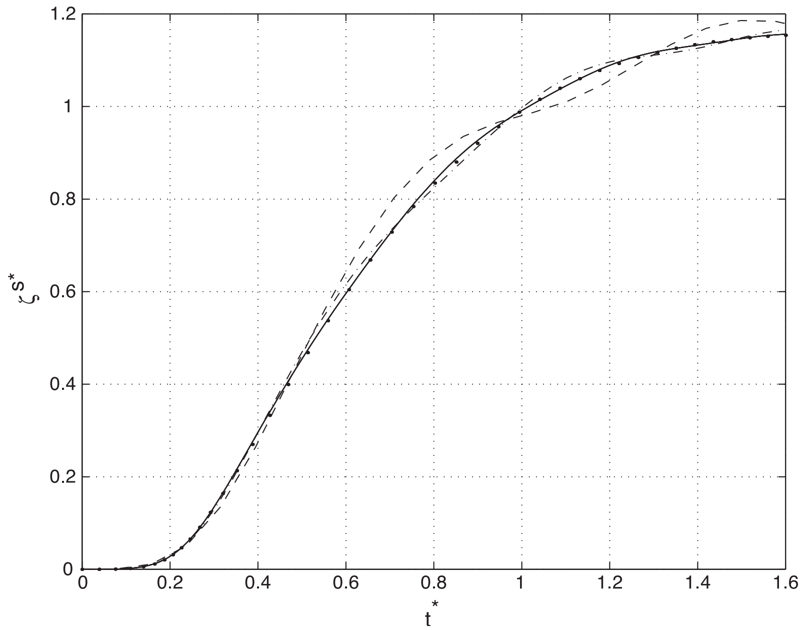

Fig. 13. Fixed grid method: time series of the surface elevation at the shoreline for the CG58's transient case for different Δx^*. The analytical solution (▪ ▪ ▪); $\Delta x^*=0.0039175$ (——); $\Delta x^*=0.007835$ (– – –); $\Delta x^*=0.01567$ (– - – - –). Courant number $Cr=0.7$ for all the cases.

accuracies similar to those found above for the fixed method with a $\Delta x^* = 0.01567$. However, though these Δx values are seemingly bigger than the values for the fixed grid method, they actually correspond to grid spacings near the shoreline, which are of the same magnitude, suggesting that near the shoreline, the two methods provide comparable accuracy. However, since the coordinate transformation method corresponds to larger grid spacing offshore, it requires a smaller number of grid points to model a domain with given accuracy at the shoreline than the number of points required with the fixed grid method.

Computations with a fixed $\Delta x^* = 0.007835$ and varying Δt^* corresponding to Courant number Cr varying in the range of 07–1.0 shows so little change with Δt^* that the results cannot be distinguished from each other or from the analytical solution.

4.1.2. Carrier and Greenspan's periodic case

CG58 also presented the analytical solution for periodic standing waves on a plane-sloping beach. For this case, the surface elevation ζ, cross-shore position x, velocity u and time t are given in the nondimensional form by

$$\zeta^* = \frac{A}{4} J_0(\sigma^*)\cos\lambda^* - \frac{u^{*2}}{2} \tag{60}$$

$$x^* = -\frac{\sigma^{*2}}{16} + \zeta^* \tag{61}$$

$$u^* = -\frac{AJ_1(\sigma^*)\sin\lambda^*}{\sigma^*} \tag{62}$$

$$t^* = \frac{1}{2}\lambda^* - u^* \tag{63}$$

This represents a wave of nondimensional frequency equal to 1, traveling towards the shore, getting fully reflected from there and creating a standing wave-like situation.

Here, A is the nondimensional wave amplitude. $A/4$ is the maximum vertical excursion of the shoreline. The above solution is valid for $0 \le A \le 1$. $A = 1$

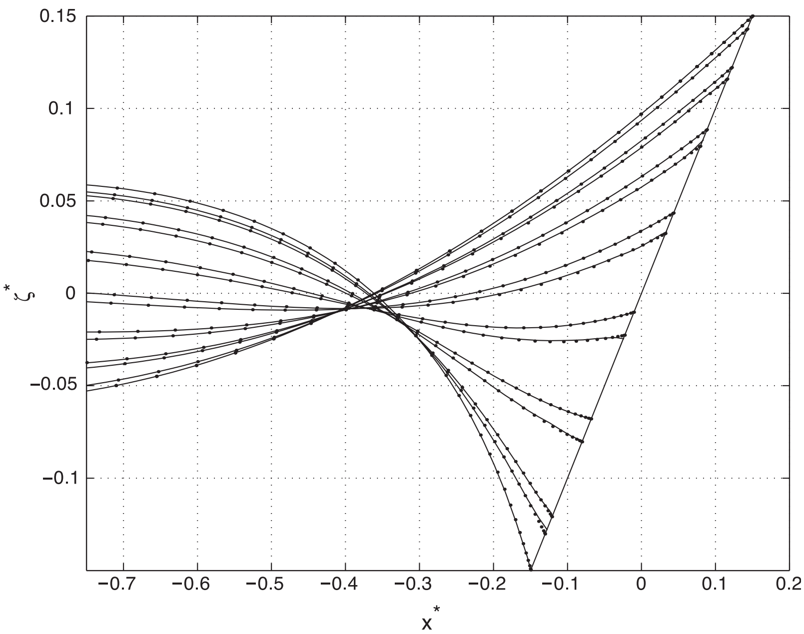

Fig. 14. The CG58's periodic case. Results from computations with a fixed grid of the surface elevation as a function of the cross-shore distance at different time steps. The analytical solution (▪ ▪ ▪); present model with fixed grid (——).

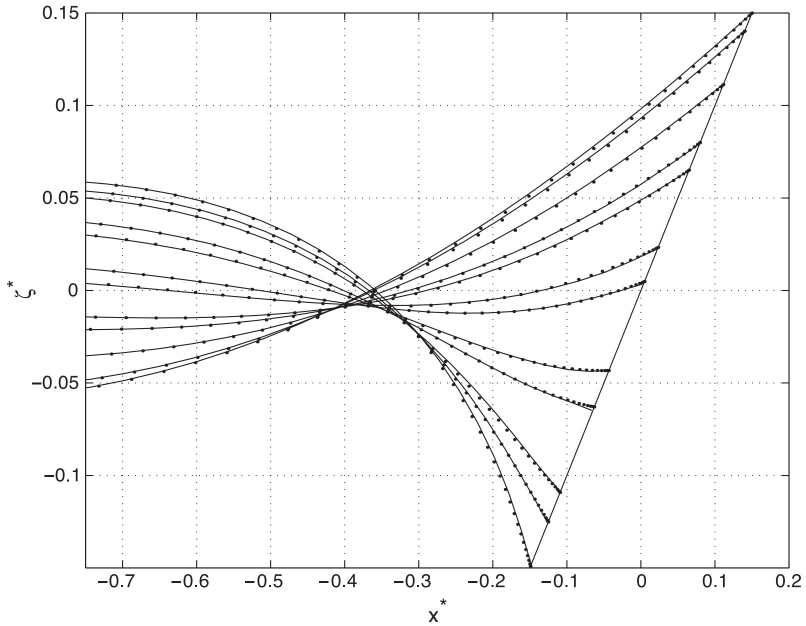

Fig. 15. Coordinate transformation model results for the surface elevation as a function of the cross-shore distance at different time steps for the periodic solution. Model (——); analytical solution (▪ ▪ ▪). $\Delta\bar{x}^* = 0.0647$ and Courant number $Cr = 0.7$ were used.

corresponds to a vertical tangent on the surface elevation. Mathematically, when $A = 1$, the Jacobian of the transformation used to arrive at these solutions becomes zero and the transformation looses the one-to-one correspondence between the actual and the transformed variables.

At $\lambda = 0$, we have $u^* = 0$ and $t^* = 0$. Therefore, the initial conditions are given here by

$$\zeta^* = \frac{A}{4} J_0(\sigma) \tag{64}$$

$$x^* = -\frac{\sigma^2}{16} + \zeta^* \tag{65}$$

and

$$u^* = 0 \tag{66}$$

The length scale $l = 20$ m and the bottom slope α was chosen to be 1/30. Results for $A = 0.6$ are presented here (Fig. 14).

Similarly for the coordinate transformation method, the initial surface profile as given by Eqs. (64) and (65) was imposed in the numerical model in the dimensional form. Again the length scale l was selected to be 20 m and the beach slope $\alpha = 1/30$. Fig. 15 shows the surface elevation as a function of the cross-shore distance at different time steps.

As mentioned, the time and grid steps of $\Delta\bar{x}^* = 0.0647$ and Courant number $Cr = 0.7$ are chosen so that the agreement is good. This result, however, is not as trivial as it may seem because particularly, the motion around the extreme downrush is very fast and can place severe strains on the accuracy of the method. Figs. 16 and 17 show the time series of the surface elevation at the shoreline for different values of Δx. We see that, again, the errors grow at a moderate and controlled rate as Δx increases.

4.2. Numerical solutions in 2DH

In the course of studying the response of harbors to long-wave excitation, Zelt (1986) developed a Lagrangian finite element model. It was

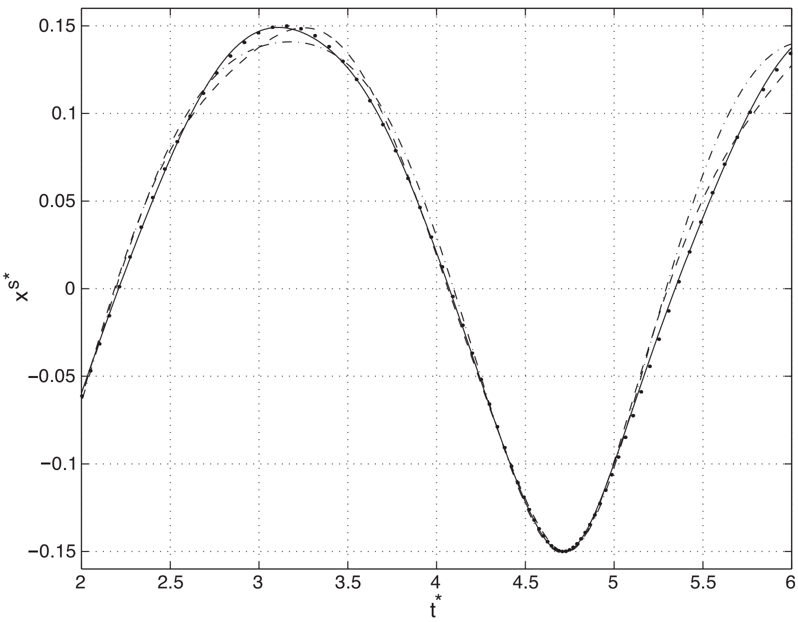

Fig. 16. The CG58's periodic case. Time series of the surface elevation at the shoreline for different Δx^* in the model with fixed grid. The analytical solution (▪ ▪ ▪); $\Delta x^* = 0.015$ (——); $\Delta x^* = 0.02$ (– – –); $\Delta x^* = 0.03$ (– - - - –). Courant number $Cr = 0.7$ for all the cases.

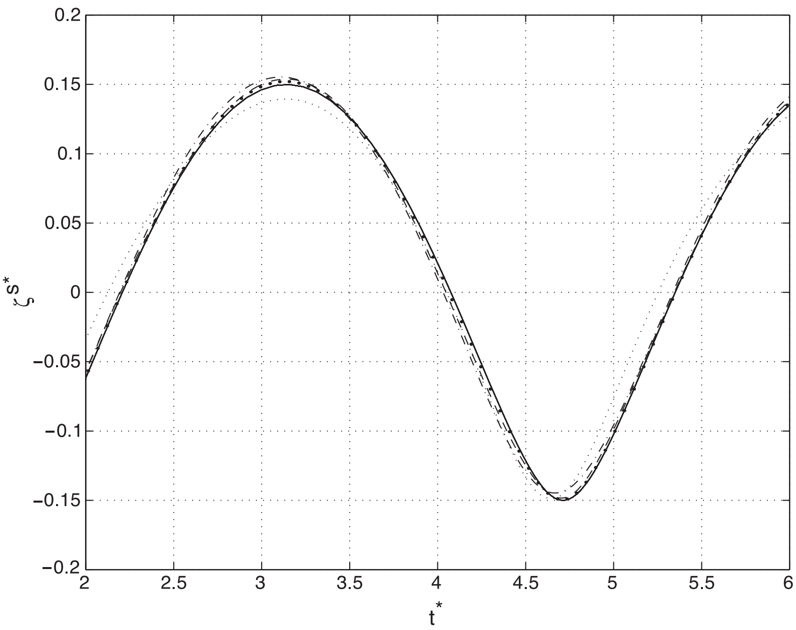

Fig. 17. CG58 periodic case. Time series of the surface elevation at the shoreline with different grid spacing in coordinate transformation model. Analytical solution (——); $\Delta \bar{x}^* = 0.032345$ (▪ ▪ ▪); $\Delta \bar{x}^* = 0.06469$ (– – –); $\Delta \bar{x}^* = 0.12938$ (– - - - –); $\Delta \bar{x}^* = 0.25876$ (- - - -). $Cr = 0.7$ for all the cases.

applied to the case of the run-up and run-down due to the incidence of a solitary wave on a beach where a curved shoreline meets a region of constant depth with a sloping bathymetry nearshore. The bottom topography is shown in Fig. 18. Such geometry was chosen to demonstrate the interaction of different processes affecting the shoreline run-up. This case is used here for comparison with the results of the coordinate transformation model in 2DH.

The undisturbed water depth, as shown in Fig. 18, is given by

$$h(x,y) = \begin{cases} h_0, & \text{for } x < L \\ h_0 - \dfrac{h_0 \pi}{L}\left[\dfrac{(x-L)}{3-\cos\left(\dfrac{\pi y}{L}\right)}\right]. & \text{for } x \geq L \end{cases} \tag{67}$$

where the length scale L is half the wavelength of the cosine form of the shoreline.

By setting $h=0$ in Eq. (67) and solving for x, the initial shoreline position can be obtained and is given by

$$x^s = L + \frac{L}{\pi}\left(3 - \cos\frac{\pi y}{L}\right) \tag{68}$$

The results of the simulations by Zelt (1986) for the topography shown in Fig. 18 were presented as the time series of the surface elevation of the shoreline at the five locations, $y/L=0$, 0.25, 0.5, 0.75 and 1, respectively, in the longshore direction and the maximum run-up and run-down as a function of the longshore position for the different values of α. Time has been nondimensionalized with a time scale $T=\sqrt{gh_0}/L$, and the nondimensional time $t=0$ is chosen as the time at which the run-up is maximum at the lateral boundaries.

Figs. 19 and 20 show the comparison of the present model results with fixed grid with the results presented by Zelt (1986) for the time series of the surface elevation at the five longshore locations and the maximum run-up and the minimum run-down as a function of the longshore position. Figs. 21 and 22

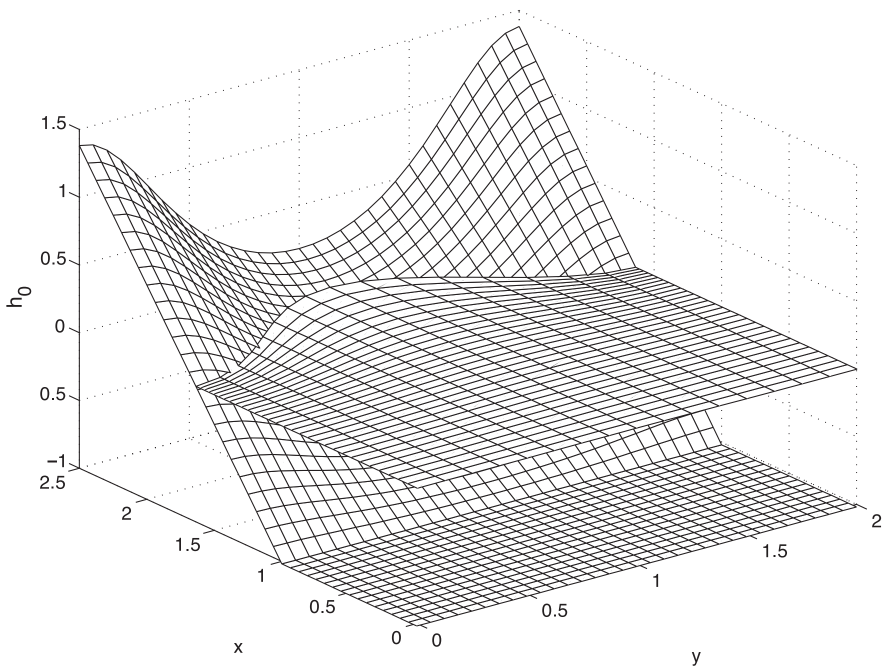

Fig. 18. Bottom topography used by Zelt (1986).

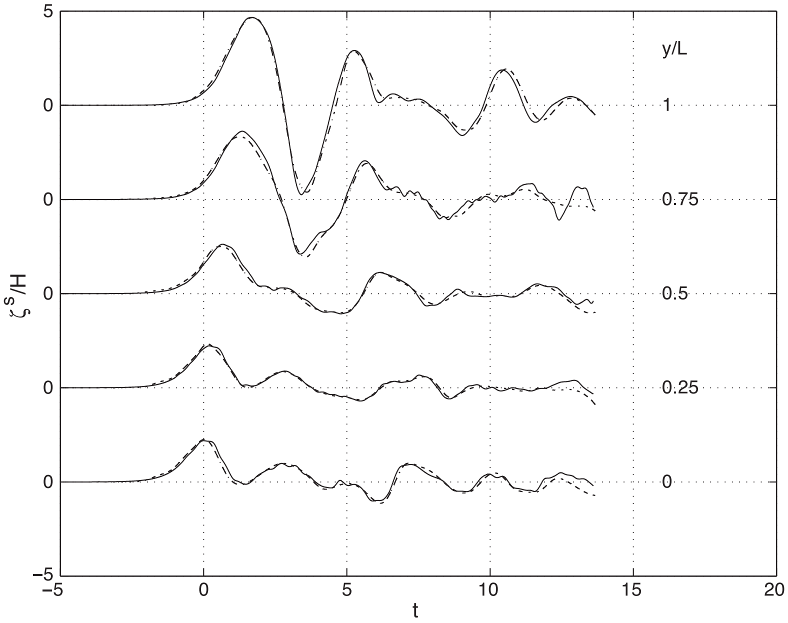

Fig. 19. Time series of the surface elevation at the shoreline. SHORECIRC with fixed grid (——); Zelt (1986) (– - - - –).

show these results with the coordinate transformation method. Özkan Haller and Kirby (1997) also used Zelt's case to test the moving shoreline boundary condition in 2DH for their Fourier–Chebyshev collocation model. Those results are also included in Figs. 21 and 22.

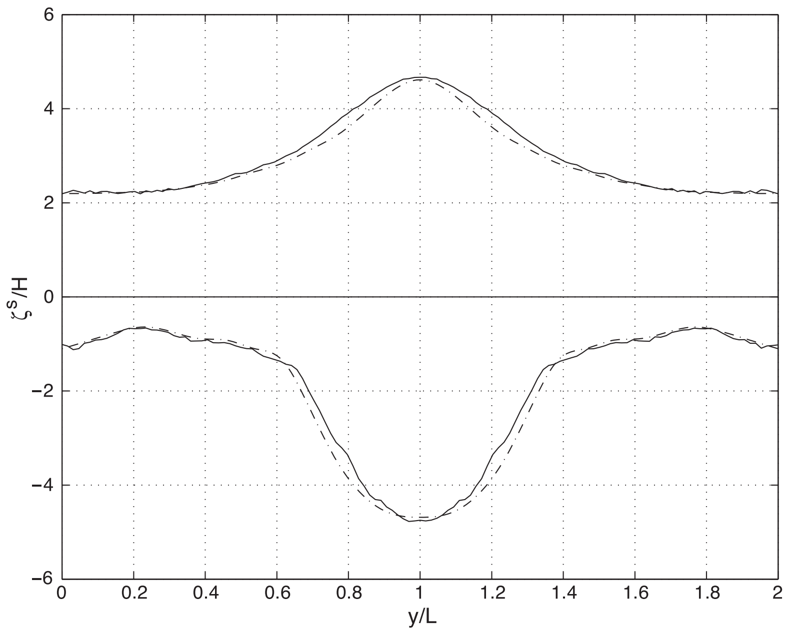

Fig. 20. The maximum run-up and the minimum run-down as a function of the longshore position. SHORECIRC with fixed grids (——); Zelt (1986) (– - - - –).

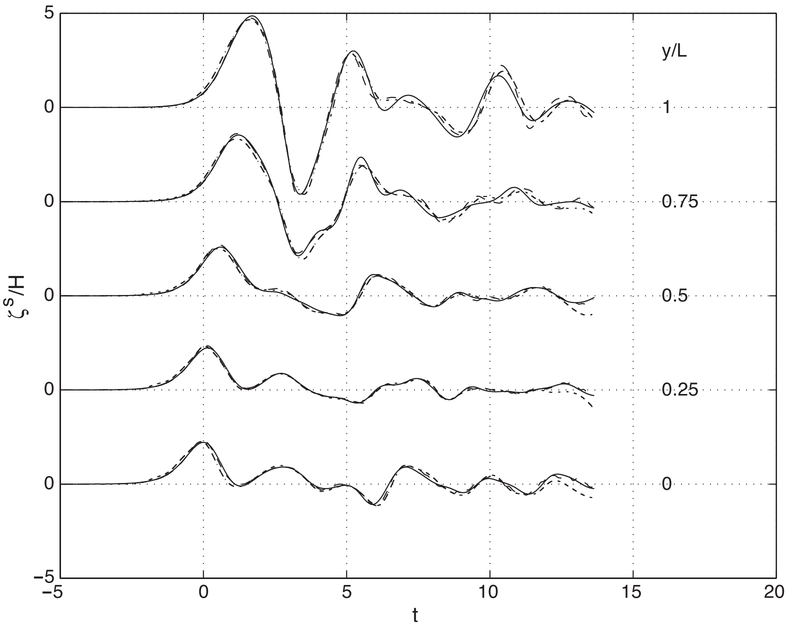

Fig. 21. Time series of the surface elevation at the shoreline along different longshore locations. The present model with coordinate transformation (——); Zelt (1986) (– - - - –); Özkan Haller and Kirby (1997) (– – –).

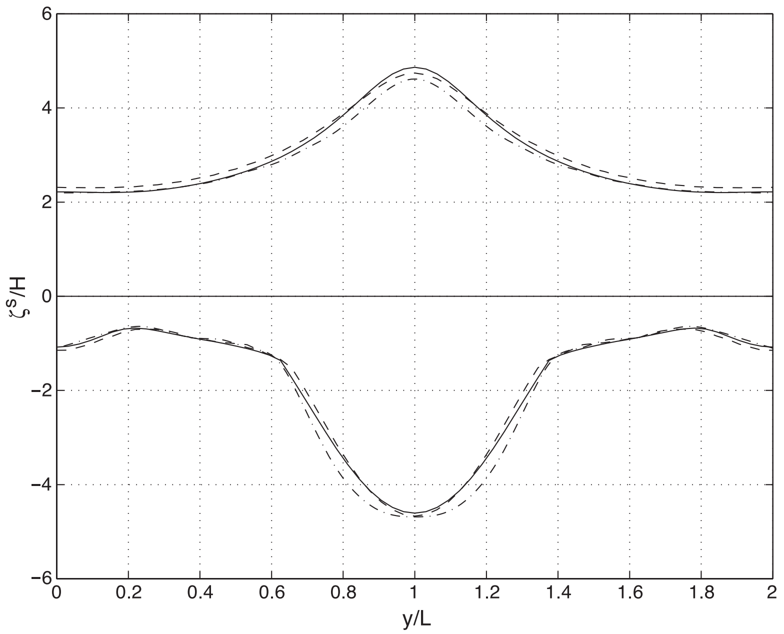

Fig. 22. The maximum run-up and the minimum run-down as a function of the longshore position. The present model with coordinate transformation (——); Zelt (1986) (– - - - –); Özkan Haller and Kirby (1997) (– – –).

5. Discussion and conclusion

As mentioned in the comparisons, the grid spacing Δx and the size of the time step Δt have been chosen so that the accuracy of the comparisons is reasonably good. For the time step, this implies a Δt that corresponds to a Courant $O(<1)$.

On one side, this means that the values of the grid spacing used for each of the two methods are an indicator of the efficiency of the method. We see that in this regard, the transformation method generally is a little more efficient than the fixed grid formulation.

At the same time, increases in the grid spacing illustrate the nature of the errors that develop if Δx is chosen larger than what good accuracy requires. These experiments indicate that the error for large Δx is benign. Errors are evenly distributed and within the range if none of the methods blow up in the grid sizes tested.

It is also observed that while both methods naturally are quite sensitive to the value of the grid size, the sensitivity to changes in the time step is not nearly as prominent.

Finally, it is noted that both methods have been tested and shown to run well on a wide range of situations ranging from the highly nonlinear 1-D horizontal cases of Carrier and Greenspan to the fully 2-D horizontal run-up of a solitary wave on a cusped beach first analyzed by Zelt. It is characteristic for all cases that the most challenging phase of the motion is the rapid changes occurring at the time of maximum downrush. There, the accelerations can become huge and if the amplitude of the imposed motion is large enough, the local surface variation at the shoreline becomes vertical. In that case, the basis for the underlying NSW equations fails and computations collapse.

While the transformation method may be more efficient, the fixed grid method is attractive in its simplicity and probably easier to fit into large-scale simulations.

Acknowledgements

The authors thank M. Brocchini and G. Belotti for inspiring discussions and comments. The work is a result of research sponsored by grant no. N00014-97-1-0791 funded by the collaborative NICOP program and by ONR grant N00014-99-1-0398 funded by the National Oceanographic Partnership Program (NOPP). The US government is authorized to produce and distribute reprints for government purposes notwithstanding any copyright notation that may appear herein.

References

Balzano, A., 1998. Evaluation of methods for numerical simulation of wetting and drying in shallow water flow models. Coastal Engineering 34, 83–107.

Brocchini, M., Peregrine, D.H., 1996. Integral flow properties of the swash zone and averaging. Journal of Fluid Mechanics 317, 241–273.

Carrier, G.F., Greenspan, H.P., 1958. Water waves of finite amplitude on a sloping beach. Journal of Fluid Mechanics 4 (1), 97–109.

DeSilva, S.J., Gunther, R.B., Hudspeth, R.T., 1996. Irregular points in 2-d free surface flows with surface tension for the wavemaker boundary value problem. Applied Ocean Research 18, 293–302.

Gopalakrishnan, T.C., Tung, C.C., 1983. Numerical analysis of a moving boundary problem in coastal hydrodynamics. International Journal of Numerical Methods in Fluids 3, 179–200.

Haas, K., Svendsen, I.A., 2000. Three dimensional modeling of rip current system. Research Report CACR-00-06. University of Delaware.

Hibberd, S., Peregrine, D.H., 1979. Surf and run-up on a beach: a uniform bore. Journal of Fluid Mechanics 95 (2), 323–345.

Jamet, P., Bonnerot, R., 1975. Numerical solution of the eulerian equations of compressible flow by finite element method which follows the free boundary and the interfaces. Journal of Computational Physics 18, 21–45.

Johns, B., 1982. Numerical integration of the shallow water equations over a sloping shelf. International Journal for Numerical Methods in Fluids 2, 253–261.

Johns, B., Dube, S.K., Sinha, P.C., Mohanty, U.C., Rao, A.D., 1982. The simulation of a continuously deforming lateral boundary in problems involving the shallow water equations. Computers and Fluids 10 (2), 105–116.

Joseph, D.D., 1973. Domain perturbation: higher order theory of infinitesimal water waves. Arch Rational Mechanics Analysis 51, 295–303.

Kobayashi, N., Otta, A.K., Roy, I., 1987. Wave reflection and run-up on rough slopes. Journal of Waterway, Port, Coastal, and Ocean Engineering 113 (3), 282–298.

Liu, P.L.-F., Cho, Y.-S., Briggs, M.J., Lu, U.K., Synolakis, C.E., 1995. Runup of solitary waves on a circular island. Journal of Fluid Mechanics 302, 259–285.

Lynch, D.R., Gray, W.G., 1980. Finite element simulation of flow in deforming regions. Journal of Computational Physics 36, 135–153.

Lynett, P.J., Wu, T.-R., Liu, P.L.-F., 2002. Modeling wave run-up with depth-integrated equations. Coastal Engineering 46, 89–107.

Militello, A., 1998. Hydrodynamics of Wind-Dominated, Shallow Embayments. PhD Thesis, Florida Institute of Technology.

Özkan Haller, H.T., Kirby, J.T., 1997. Nonlinear evolution of the shear instabilities of the longshore current. Research Report CACR 97-08. University of Delaware.

Pedersen, G., Gjevik, B., 1983. Run-up of solitary waves. Journal of Fluid Mechanics 135, 283–299.

Reid, R.O., Bodine, B.R., 1968. Numerical model for storm surges in Galveston Bay. Journal of the Waterways and Harbors Division 94 (WW 1), 33–57.

Sancho, F., Svendsen, I.A., 1997. Unsteady nearshore currents on longshore varying topographies. Research Report CACR-97-10. University of Delaware.

Shi, F., Sun, W., 1995. A variable boundary model of storm surge flooding in generalized curvilinear grids. International Journal for Numerical Methods in Fluids 21, 641–651.

Sielecki, A., Wurtele, M.G., 1970. The numerical integration of the nonlinear shallow water equations with sloping boundaries. Journal of Computational Physics 6, 219–236.

VanDongeren, A.R., Svendsen, I.A., 1997. Quasi 3-d modeling of nearshore hydrodynamics. Research Report CACR-97-04. University of Delaware.

Zelt, J.A., 1986. Tsunamis: the response of harbours with sloping boundaries to long wave excitation. Technical Report KH-R-47. California Institute of Technology, Pasadena, California.

Zelt, J.A., 1991. The run-up of nonbreaking and breaking solitary waves. Coastal Engineering 15, 205–246.

Zelt, J.A., Raichlen, F., 1990. A Lagrangian model for wave induced harbor oscillation. Journal of Fluid Mechanics 213, 203–225.